University of Pennsylvania
ScholarlyCommons

Departmental Papers (MEAM)

Department of Mechanical Engineering & Applied Mechanics

September 2002

A stirrer for magnetohydrodynamically controlled minute fluidic networks

Shizhi Qian
University of Pennsylvania

Jianzhong Zhu
University of Pennsylvania

Haim H. Bau
University of Pennsylvania, bau@seas.upenn.edu

Follow this and additional works at: http://repository.upenn.edu/meam_papers

A stirrer for magnetohydrodynamically controlled minute fluidic networks

Abstract

Magnetohydrodynamics may potentially provide a convenient means for controlling fluid flow and stirring fluids in minute fluidic networks. The branches of such fluidic networks consist of conduits with rectangular cross sections. Each conduit has two individually controlled electrodes positioned along opposing walls and additional disk-shaped electrodes deposited in the conduit's interior away from its sidewalls. The network is positioned in a uniform magnetic field. When one applies a potential difference between a disk-shaped electrode and two wall electrodes acting in tandem, circulatory motion is induced in the conduit. When the potential difference alternates periodically across two or more such configurations, complicated (chaotic) motions evolve. As the period of alternation increases, so does the complexity of the flow. We derive a two-dimensional, time-independent expression for the magnetohydrodynamic creeping flow around a centrally positioned disk-shaped electrode in the limit of zero radius. With the aid of this expression, the trajectories of passive tracers are computed as functions of the alternations protocol and the electrodes' locations. The theoretical results are qualitatively compared with flow visualization experiments.

A stirrer for magnetohydrodynamically controlled minute fluidic networks

Shizhi Qian, Jianzhong Zhu, and Haim H. Bau[a]

Department of Mechanical Engineering and Applied Mechanics, University of Pennsylvania, Philadelphia, Pennsylvania 19104-6315

Magnetohydrodynamics may potentially provide a convenient means for controlling fluid flow and stirring fluids in minute fluidic networks. The branches of such fluidic networks consist of conduits with rectangular cross sections. Each conduit has two individually controlled electrodes positioned along opposing walls and additional disk-shaped electrodes deposited in the conduit's interior away from its sidewalls. The network is positioned in a uniform magnetic field. When one applies a potential difference between a disk-shaped electrode and two wall electrodes acting in tandem, circulatory motion is induced in the conduit. When the potential difference alternates periodically across two or more such configurations, complicated (chaotic) motions evolve. As the period of alternation increases, so does the complexity of the flow. We derive a two-dimensional, time-independent expression for the magnetohydrodynamic creeping flow around a centrally positioned disk-shaped electrode in the limit of zero radius. With the aid of this expression, the trajectories of passive tracers are computed as functions of the alternations protocol and the electrodes' locations. The theoretical results are qualitatively compared with flow visualization experiments. © *2002 American Institute of Physics.* [DOI: 10.1063/1.1504713]

I. INTRODUCTION

In recent years, there has been a growing interest in developing minute fluidic systems for biodetection, biotechnology, chemical reactors, and medical, pharmaceutical, and environmental monitoring. In many of these applications, it is necessary to propel fluids from one part of the device to another, control the fluid motion, stir, and separate fluids. In minute devices, these tasks are far from trivial. Typically, electrostatic forces are being used to move liquids around. However, these forces usually induce very low flow rates and require the use of very high electric fields.

The application of electromagnetic forces to pump, confine, and control fluids is by no means new. To date, however, magnetohydrodynamics (MHD) has mostly been used to pump and control highly conducting fluids such as liquid metals and ionized gases and to study ionospheric/astrophysical plasmas.[1,2] The potential use of electromagnetic forces in microdevices has attracted much less attention. Recently, though, various groups[3–5] constructed MHD micropumps on silicon and ceramic substrates and demonstrated that these pumps are able to move liquids around in microconduits. The liquids need to be only slightly conductive—a requirement met by many biological solutions.

Subsequently, Bau[6] demonstrated the feasibility of using magnetohydrodynamic (MHD) forces to control fluid flow in minute fluidic networks. The basic building block (branch) of such a network is depicted in Fig. 1. The branch consists of a conduit with two electrodes (C^+ and C^-) deposited along its two opposing walls. The conduit is filled with an electrolyte solution. Many conduits of the type depicted in Fig. 1 can be connected to form a network. The entire device is subjected to a uniform magnetic field in the z direction. When a potential difference is applied across the electrodes C^+ and C^-, the resulting current interacts with the magnetic field to form body (Lorentz) forces that propel the fluid. By judicious application of different potential differences to different electrode pairs, one can direct the liquid to flow along any desired path without a need for mechanical pumps and valves.[6] In other words, MHD allows us to control fluid flow in the minute fluidic network in very much the same way as one controls electric current flow in an electronic circuit.

In this paper, we demonstrate that the basic network elements can perform yet another important task—that of stirring. In order to facilitate chemical reactions and biological interactions, it is necessary to bring various molecules together. Diffusion alone is far too slow to achieve this task. Since the Reynolds numbers of flows in microdevices are usually very small, one is denied the benefits of turbulence as an efficient mixer. However, since one can readily pattern electrodes of various shapes, one can induce electric fields in different directions. The interaction of such electric fields with the magnetic field can be used to induce secondary complex flows that may be beneficial for stirring and mixing. The feasibility of inducing such secondary flows, including chaotic flows, was demonstrated in Bau, Zhong, and Yi[7] and Yi, Qian, and Bau[8] (to which we refer hereafter as YQB). For example, the latter paper describes a stirrer consisting of a closed cylindrical cavity with an electrode (C) deposited around its periphery and two additional electrodes A and B deposited eccentrically inside the cavity on the cavity's bottom. Chaotic advection was obtained by alternating the elec-

---

Phys. Fluids, Vol. 14, No. 10, October 2002
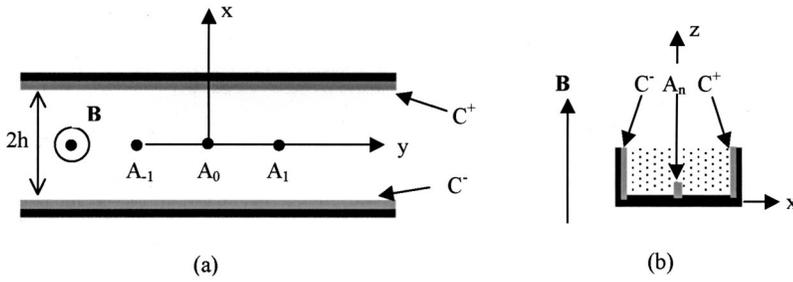
A MHD chaotic stirrer for fluidic networks   3585

FIG. 1. A liquid-filled conduit is confined between two parallel plates ($x = \pm h$). A uniform magnetic field, B, is parallel to the z coordinate. Electrodes C^+ and C^- are deposited along the confining plates ($x = \pm h$) and "point" electrodes A_{-1}, A_0, and A_1 are positioned along $x = 0$, distance c apart. When the device operates as a stirrer, electrodes C^+ and C^- are wired to act in tandem as a single electrode C. (a) Top view; (b) side view.

tric potential difference across electrodes $A-C$ and $B-C$. Such a stirrer is not suitable, however, when one desires to facilitate through flow.

In this paper, we describe a variant of YQB's stirrer that is better suited for integration into the MHD network. Only slight modifications are needed in the network's branches so that they can serve the double function of a "pump" and a "stirrer." To this end, we deposit point electrodes (denoted A_n in Fig. 1) along the centerline of the conduit's bottom. When we wish the network branch to operate as a stirrer, we connect both electrodes C^+ and C^- to the same terminal of a power supply so that they act in tandem as the single electrode C. When a potential difference is imposed across any of the central electrodes A_n and the electrode C, circulatory motion ensues with the liquid circulating around the electrode A_n. When two or more internally positioned electrodes are alternately actuated, complex, chaotic flows are induced. This arrangement is similar to Aref's[9] blinking vortex. In contrast to Aref's highly idealized, inviscid system, the stirrer studied here can be readily constructed. Our paper is yet another example of Stokes flow that exhibits chaotic advection. The literature on chaotic Stokes flows is quite extensive, and additional relevant papers are cited in YQB. The most relevant paper to our study is the work of Hackborn et al. on chaotic advection in Stokes flow between long, parallel plates.[10] The flow is driven by the rotation of a confined cylinder and longitudinal oscillation of one of the confining plates. In contrast, our stirrer does not require any moving parts.

This paper is organized as follows. We first derive a singular solution for the magnetohydrodynamic, creeping flow between long parallel planes for the special case when the radius of the inner electrode shrinks to zero. Subsequently, using a quasistatic approximation, we compute the flow field and the trajectories of passive tracers when two or more centrally located (A_n) electrodes are actuated alternately. Not surprisingly, as the period of the modulations increases so does the complexity of the flow. Finally, the theoretical predictions are qualitatively compared with experimental observations.

II. MATHEMATICAL MODEL: STEADY FLOW

In this section, we describe a somewhat idealized two-dimensional model of the MHD stirrer. Such a model is necessitated by our need for a relatively simple and accurate expression for the flow field in order to enable the study of chaotic advection. Despite its simplicity, the model gives a qualitatively reasonable description of the phenomena that occur in experiments.

Consider two long parallel plates ($x = \pm h$) placed distance $2h$ apart (Fig. 1). Electrodes C^+ and C^- are deposited along these plates. The electrodes are wired to act in tandem as a single electrode C that is connected to one terminal of a power supply. Additional "point" electrodes A_n ($n = 0, \pm 1, \pm 2, ...$) are located middistance between C^+ and C^- and placed distances (c) apart. In other words, the point electrodes (A_n) are located at $(x,y) = (0, nc)$. The conduit is filled with at least weakly conducting liquid of electrical conductivity (σ) and viscosity (μ). A potential difference ΔV is imposed between one of the central electrodes (A_n) and electrode C. The conduit is placed in a uniform, static magnetic field of flux density $\mathbf{B} = B\hat{e}_z$ directed in the (z) direction. We use bold letters to denote vectorial quantities.

According to Ohm's law for a moving conductor of conductivity σ in a magnetic field, the potential difference ($\Delta V = V_1 - V_2$) induces a current of density:

$$\mathbf{J} = \sigma(-\boldsymbol{\nabla} V + \mathbf{u} \times \mathbf{B}). \tag{1}$$

In Eq. (1), $\mathbf{u}$ is the fluid's velocity. The interaction between the electric current and the magnetic field generates a (volumetric) Lorentz force of density $\mathbf{J} \times \mathbf{B}$. For a two-dimensional, incompressible flow, the momentum equation is

$$\rho \frac{D\mathbf{u}}{Dt} = \mathbf{J} \times \mathbf{B} - \boldsymbol{\nabla} p + \mu \nabla^2 \mathbf{u}, \tag{2}$$

where t is time, p is the pressure, and ρ is the liquid's density. We nondimensionalize all quantities using (h) as the length scale; $U = BI'h/2\pi\mu$ as the velocity scale; h/U as the time scale; $BI'/2\pi$ as the pressure scale; and $I'/2\pi\sigma$ as the electric potential scale. In the above, I' is the electric current per unit depth (in the z direction). The dimensionless momentum equation assumes the form

$$\mathrm{Re} \frac{\partial \mathbf{u}}{\partial t} = (-\boldsymbol{\nabla} V + Ha^2 \mathbf{u} \times \hat{\mathbf{e}}_z) \times \hat{\mathbf{e}}_z - \boldsymbol{\nabla} p + \nabla^2 \mathbf{u}, \tag{3}$$

where $\hat{\mathbf{e}}_z$ is a unit vector in the z direction.

In Eq. (3), we neglected advection, assuming that the Reynolds number ($\mathrm{Re} = Uh/\nu$) is small. Later, we will also assume that the ratio between the convective time scale and the time modulations of the electric field (T^*) is $h/(UT^*)$ $\ll 1$, that the flow is quasistatic, and that the time derivative can be neglected.[11] $Ha = Bh\sqrt{(\sigma/\mu)}$ is the Hartman number. When the liquid is a weak conductor of electricity such as in

the case of saline solutions, the Hartman number is small and the term $\mathbf{u} \times \hat{\mathbf{e}}_z$ can be safely neglected. For example, in our case, $\text{Ha} \sim O(10^{-2})$:

The electric potential (V) satisfies the Laplace equation:

$$\nabla^2 V = 0. \tag{4}$$

The solution of the Laplace equation can be readily obtained utilizing Log–Tan–Cylinder coordinates.[12,13] Here we consider the limiting case when the inner electrode A_n shrinks to the point $(0,n\,c)$. More specifically, as the radius of the electrode decreases, the potential difference ΔV increases so as to maintain a fixed current. Accordingly, V satisfies the following boundary conditions:

$$V(\pm 1, y) = V(x, \pm \infty) = 0 \quad \text{and} \quad \lim_{y \to nc} V(0,y) \to \infty. \tag{5}$$

Equations (4) and (5) admit the solution[12]

$$V(x,y) = \ln(F(x,y)), \tag{6}$$

where

$$F(x,y) = \frac{1 - 2\exp\left(\dfrac{\pi(y-nc)}{2}\right)\cos\left(\dfrac{\pi x}{2}\right) + \exp(\pi(y-nc))}{1 + 2\exp\left(\dfrac{\pi(y-nc)}{2}\right)\cos\left(\dfrac{\pi x}{2}\right) + \exp(\pi(y-nc))}. \tag{7}$$

It is convenient to introduce the stream function ψ such that $u_x = \partial \Psi / \partial y$ and $u_y = -\partial \Psi / \partial x$. The dimensionless steady-state momentum equations,

$$\frac{\partial}{\partial y}(\nabla^2 \Psi + V) = \frac{\partial p}{\partial x},$$

$$-\frac{\partial}{\partial x}(\nabla^2 \Psi + V) = \frac{\partial p}{\partial y}, \tag{8}$$

with the boundary conditions,

$$\Psi(\pm 1, y) = \frac{\partial \Psi(\pm 1, y)}{\partial x} = \Psi(x, \pm \infty) = \frac{\partial \Psi(x, \pm \infty)}{\partial y} = 0, \tag{9}$$

admit the solution

$$\Psi_n(x,y) = -\frac{x^2 + (y-nc)^2}{4}\ln[F(x,y)]$$

$$-\int_0^\infty h(x,k)\cos[k(y-nc)]dk. \tag{10}$$

In the above,

$$h(x,k) = \frac{\sec h^2(k)[\tanh(k)\cosh(kx) - x\sinh(kx)]}{k + \cosh(k)\sinh(k)}. \tag{11}$$

Both terms in (10) satisfy the biharmonic equation. The second term is a Fourier integral that was introduced to satisfy the boundary conditions at $x = \pm 1$. As $|y| \to \infty$, the first term decays like $y^2 \exp(-\pi|y|/2)$. The integrand decays rapidly (like e^{-3k}).

Equation (10) is a new singular solution for the two-dimensional, magnetohydrodynamic Stokes problem for a point electrode confined between two parallel planes (elec-
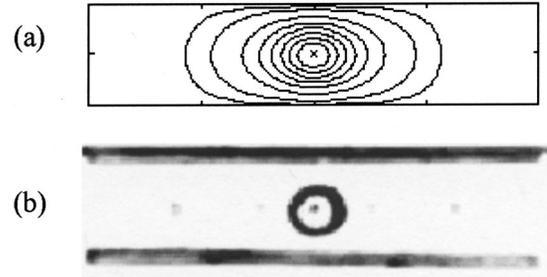

FIG. 2. The flow field induced by a single electrode group $A_0 - C$. (a) Computed streamlines. (b) Flow visualization photograph.

trodes). Figures 2(a) and 2(b), respectively, depict the computed and experimentally observed flow fields when $n = 0$. The experimental setup is described later in the paper. The flow visualization was carried out by dye injection. The flow circulates around the electrode with an elliptic fixed (stagnation) point at the electrode's location. The MHD flow topology is quite different from the flow field induced by a rotlet confined between two parallel plates.[13] In the case of the rotlet, the flow consists of an infinite sequence of Moffatt[14] eddies. The existence of an angular Lorentz force precludes the formation of such eddies in our case.

Figure 3 depicts the velocity profiles $u_y(x,0)$ and $u_x(0,y)$. The velocity decreases rapidly (exponentially) as $|y|$ increases. This is consistent with the exponential decrease in the current's density as one moves away from A_0. Although the above-described flow serves to move liquid transversely across the width of the conduit, the motion is quite regular, and the stirring is not very efficient. In order to improve the efficiency of the stirring, we alternate the potential difference across a few groups ($A_n - C$) of electrodes.

III. TIME-MODULATED FLOWS

In this section, we study the chain of events when the potential difference is alternated across two, i.e., $A_{-1} - C$ and $A_1 - C$, and three, i.e., $A_{-1} - C$, $A_0 - C$, and $A_1 - C$, configurations. If one so desires, a larger number of electrode groups can be engaged. When we engage two electrode groups, we impose a potential difference across $A_{-1} - C$ for the time interval $0 < t < T_1$ and then a potential difference of the same magnitude (albeit not necessarily the same polarity) across $A_1 - C$ for the time interval $T_1 < t < T$. Subsequently, the process is repeated with period T. Similarly, when we utilize three electrode groups, we impose the same potential differences across $A_{-1} - C$, $A_0 - C$, and $A_1 - C$ for the time intervals $0 < t < T_1$, $T_1 < t < T_2$, and $T_2 < t < T$, respectively. Subsequently, the process is repeated. Of course, one can use other algorithms as well. The choice of the algorithm that provides the most efficient stirring process is an interesting optimization problem that we do not address here.

We assume that the Reynolds number is small and the potential alternations are sufficiently slow so that the flow can be approximated as quasistatic. We also assume that the instantaneous flow field is given by the steady-state solution
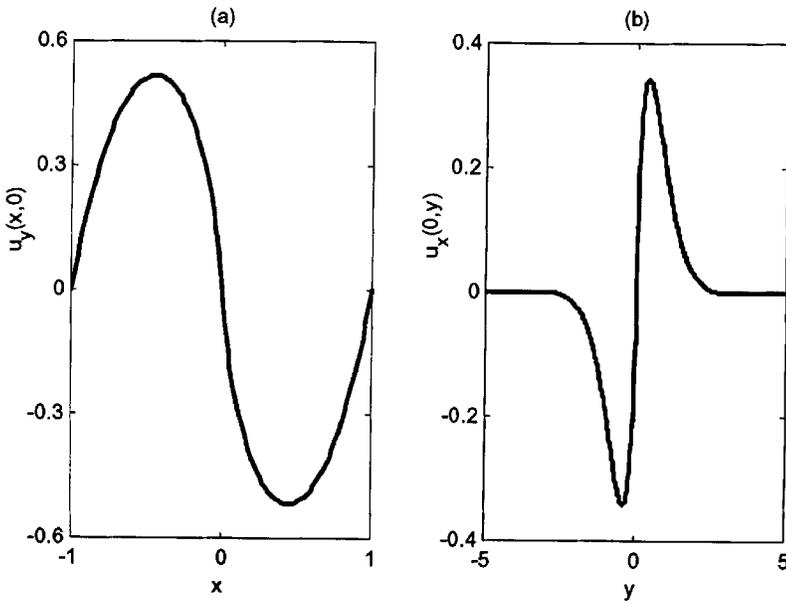
FIG. 3. Velocity profiles of flow induced by a single electrode group A_0-C. (a) $u_y(x,0)$ as a function of x; (b) $u_x(0,y)$ as a function of y.

of the Stokes equation. The approximation is commonly used in the context of Stokes flows and chaotic advection.[15,16]

When the potential difference is induced across electrode group A_n-C, we denote the resulting flow field as ψ_n [Eq. (10)]. When the potential difference alternates among electrode groups $A_{-1}-C$, A_0-C, and A_1-C while A_{-1}, A_0, and A_1 have the same polarity, the resulting flow field is

$$\psi(x,y,t) = \psi_{-1}(x,y)f_{-1}(t) + \psi_0(x,y)f_0(t)$$
$$+ \psi_{+1}(x,y)f_1(t) \qquad (12)$$

provided that no two electrode groups are engaged simultaneously, i.e., $f_0(t)=f_1(t)=0$ when $f_{-1}(t)\neq 0$. Simultaneous engagement of more than one electrode group will alter the electric field and render Eq. (10) invalid. When electrodes A_n-C ($n=-1,0,1$) are subjected to different polarities, the various electrode groups induce motion in opposite directions, and the "$+$" sign in (12) is replaced with a "$-$" sign. When we alternate only the two electrodes A_{-1} and A_1, $f_0(t)=0$.

The trajectories of passive tracers can be readily computed by numerically integrating the advection equations:

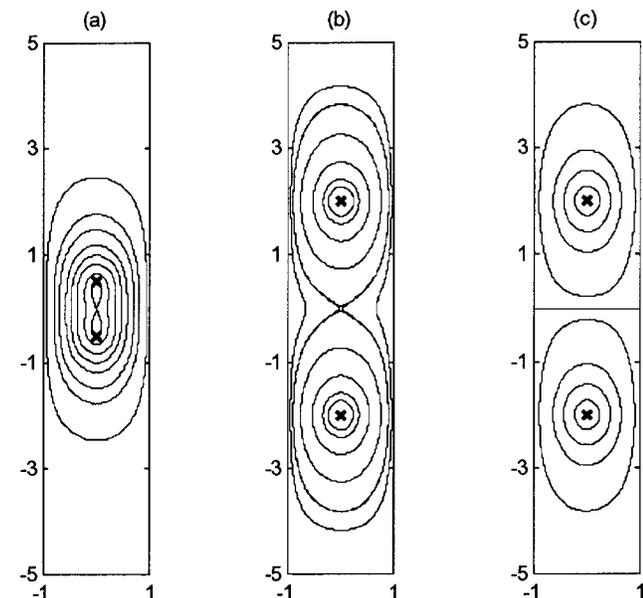

FIG. 4. Superposed flow fields in the limit of $T \rightarrow 0$ when two electrode groups ($A_{-1}-C$ and A_1-C) are alternately activated. The symbol ($\times$) denotes the positions of the "point" electrodes: (a) co-rotating and $c=0.5$; (b) co-rotating and $c=2$; (c) counter-rotating and $c=2$.
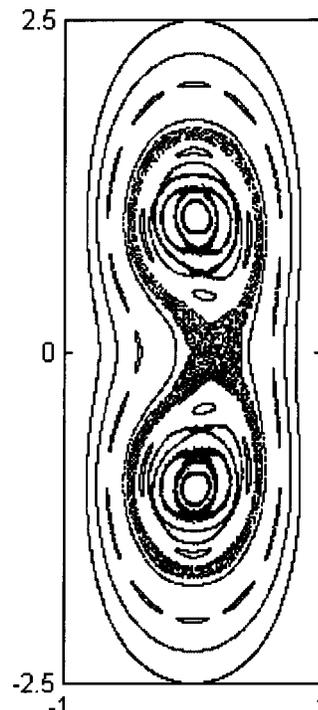

FIG. 5. Stroboscopic image (Poincaré section) when two (co-rotating) electrode groups are engaged. $c=1$, $T=4$, and $T_1=T/2$. At $t=0$, passive tracers were inserted at (0, 0), (0, ± 0.45), (0, ± 0.6), (0, ± 0.8), (0, ± 0.9), (0, 1.75), (0, 2), (0, 2.25), and (0, 2.5).
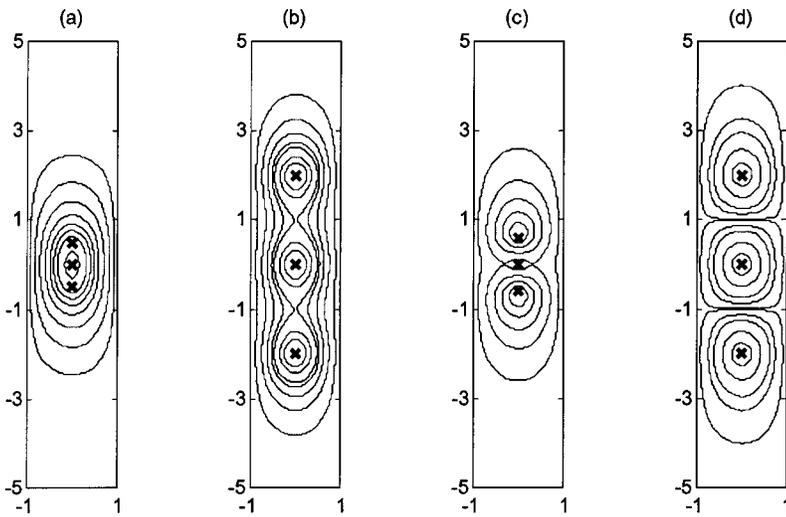
FIG. 6. Superposed flow fields in the limit of $T \to 0$ when three evenly spaced electrode groups, ($A_{-1}-C$, A_0-C, and A_1-C), are alternately engaged. The ($\times$) denotes the positions of the "point" electrodes: (a) co-rotating, $c=0.5$; (b) co-rotating, $c=2$; (c) counter-rotating, $c=0.6$; and (d) counter-rotating, $c=2$.

$$\dot{x} = u_x(x,y,t), \quad \dot{y} = u_y(x,y,t). \tag{13}$$

We computed the particles' trajectories by integrating the above-mentioned equations using Matlab's fourth-order Runge–Kutta algorithm. We were particularly interested in constructing stroboscopic images (Poincaré sections) that describe the location of the tracer at the beginning of each period, i.e., $\mathbf{x}(kT)$, where $k=0,1,2,...$ and $\mathbf{x}=\{x,y\}$. In other words, the Poincaré section maps the position of a particle at time $t(\bmod T)$ to its position one period later, $\mathbf{x}(kT) \to \mathbf{x}((k+1)T)$. Since the flow is incompressible, the map preserves area.

One can explore various types of time modulations [various functions $f_n(t)$]. Here, for brevity, we select the simple on–off protocol. The resulting flow field is periodic in time with periodicity T, i.e., $\psi(x,y,t+T) = \psi(x,y,t)$. The "on–off" potocol is not quite consistent with the Stokes approximation that requires the time constant associated with the modulations to be larger than the viscous time constant. Aref and Balachandar[15] have, however, investigated the effects of various protocols on the kinematics of the flow between two rotating, eccentric cylinders and determined that an "on–off" protocol gives qualitatively indistinguishable results compared to ones obtained with "smoother" protocols. Indeed, a function $f(t)$ that provides a more gradual time-wise

change will only modify the "effective" time interval T_n without changing the qualitative nature of the flow. Within each time interval, the passive tracer's trajectory coincides with the streamlines depicted in Fig. 2. Choosing a different $f(t)$ would merely have the effect of changing the length of the segment that a particle travels along a streamline in the allotted time. In fact, we can introduce a new time-variable, $\tau = \int^t f(\xi)d\xi$, to eliminate the explicit dependence on the particular choice of $f(t)$. Finally, we note that the more interesting flow phenomena occur when (T) is relatively large and when the quasistatic approximation is likely to be valid.

We emphasize again that the expressions for the flow fields are valid when *only* one electrode A_n is active at any given time. Nevertheless, it is instructive to examine the flow field in the limiting case of the alternations period, $T \to 0$. We think of T as a "control" parameter and follow the chain of events as T increases. When $T \to 0$, the streamlines associated with various electrode groups are simply superposed. This superposition reveals the existence of hyperbolic and elliptic, fixed (stagnation) points that have a profound effect on the evolution of the flow as T increases. Moreover, as we will see later, both in experiment and theory, when T is small, the passive tracers' trajectories follow closely the superposed flow field.

Figure 4 depicts the streamlines for a few cases when two electrode groups are engaged and $T=0$. In Figs. 4(a) and 4(b), the electrodes A_{-1} and A_1 are located, respectively, distances 1 and 4 apart and have the same polarity. Witness the presence of one hyperbolic fixed-point midway between the two electrodes A_{-1} and A_1 and two elliptic fixed points next to the electrodes A_{-1} and A_1. The qualitative features of Figs. 4(a) and 4(b) appear to be independent of the distance between the electrodes. The flow field consists of periodic orbits (tori) of periods (Γ) ranging from 0 to infinity. There are two types of orbits: orbits that encircle only one of the elliptic fixed points and orbits that encircle both elliptic points. These two families of tori are separated by homoclinic orbits that pass through the hyperbolic (saddle) point. The flow topology changes considerably when the two inner electrodes, A_{-1} and A_1, have opposing polarities [Fig.
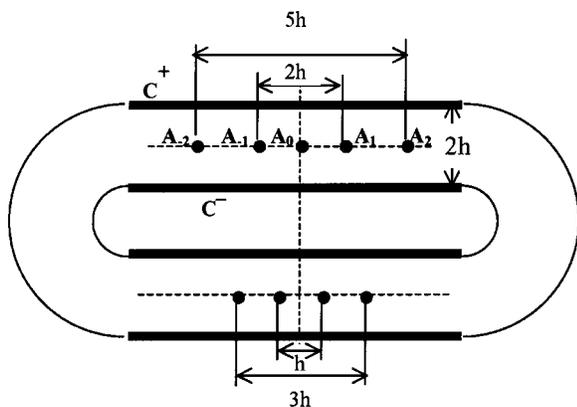

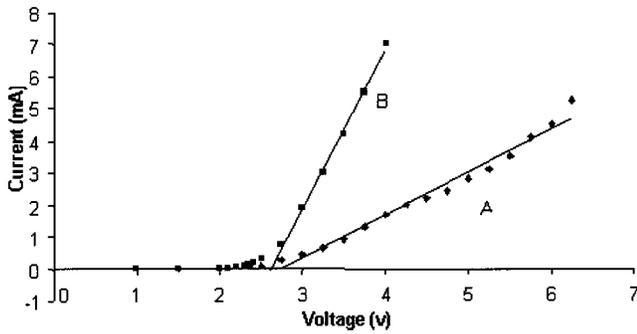FIG. 7. Schematic description of the experimental device.

FIG. 8. The electric current as a function of applied voltage. Graphs (a) and (b) correspond, respectively, to 0.1 M±10% and 0.36 M±10% NaCl solution in water.

4(c)]. In this case, the two electrode groups induce counter-rotating vortices separated by the streamline $\Psi(x,0)=0$. Each family of streamlines is centered about an elliptic, fixed point located in the vicinity of electrodes A_{-1} and A_1.

When $T=0$, the system is autonomous and integrable. When $T>0$, the system may no longer be integrable. Chaotic behavior may arise both because of the disruption of the hyperbolic fixed point and the perturbation of the tori. This process is illustrated in Fig. 5. Figure 5 depicts the stroboscopic image (Poincaré section) of the passive tracer particles' trajectories. The "particles" were initially inserted at $(0,0)$, $(0,\pm0.45)$, $(0,\pm0.6)$, $(0,\pm0.8)$, $(0,\pm0.9)$, $(0,1.75)$, $(0,2)$, $(0,2.25)$ and $(0,2.5)$ when $T=4$, $c=1$, $T_1=T/2$ and two electrode groups, $A_{-1}-C$ and A_1-C, are engaged. Both A_{-1} and A_1 have the same polarity. Witness the emergence of a chaotic region resulting from the homoclinic tangle and the formation of new hyperbolic and elliptic points.

More complicated flow topologies can form when more than two electrode groups are engaged. Figure 6 depicts a few examples when three electrode groups (A_{-1}, A_0, and A_1) are engaged. In Figs. 6(a) and 6(b), all the "point" electrodes have the same polarity. In Figs. 6(c) and 6(d), the central electrode A_0 has a different polarity than the two other electrodes (A_{-1} and A_1). In addition to its dependence

on the electrodes' polarity, the flow field's topology also depends on the distance between the electrodes. When all three "point" electrodes have the same polarity and the distances between the electrodes are relatively small [Fig. 6(a), $c<1$], all the streamlines encircle the elliptic point located at A_0. When the distances between the electrodes are increased ($c>1$), one observes the presence of two hyperbolic and three elliptic fixed points. One would expect that the presence of multiple hyperbolic points would lead to an efficient stirring process. The situation is quite different when the polarity of the electrode A_0 differs from that of the other two "point" electrodes [Figs. 6(c) and 6(d)]. When the separation between the electrodes is relatively small [Fig. 6(c)], one observes the presence of three elliptic, fixed points and two hyperbolic points. Some of the streamlines encircle only one of the three "point" electrodes while other streamlines encircle all three "point" electrodes. As the distance between the electrodes increases, the two hyperbolic, fixed points migrate toward the sidewalls ($x=\pm1$). When $c>1$ [Fig. 6(d)], these two hyperbolic points anchor on the sidewalls ($x=\pm1$), and three separate families of streamlines form. A variety of other flow structures (which we do not describe here) can be formed by adding additional electrodes and by varying the distances between the electrodes. In Sec. V, we will describe the chain of events as the period T increases.

IV. FLOW VISUALIZATION EXPERIMENTS

To illustrate that similar flows to the ones predicted can be observed in practice, we fabricated a prototype of a MHD stirrer with low temperature, co-fired ceramic tapes.[17] Figure 7 depicts schematically the experimental device. To facilitate easy flow visualization, the device was made relatively "large." The conduit's half width and depth were, respectively, $h=4$ and 2 mm. The device consisted of two 32-mm-long, straight conduit segments connected with semicircular arcs on both ends. Electrodes C^+ and C^-, made of DuPont 6146 gold paste, were printed along the walls of the straight segments. Five "point" electrodes with radii of approximately 0.3 mm were printed along the centerline of the
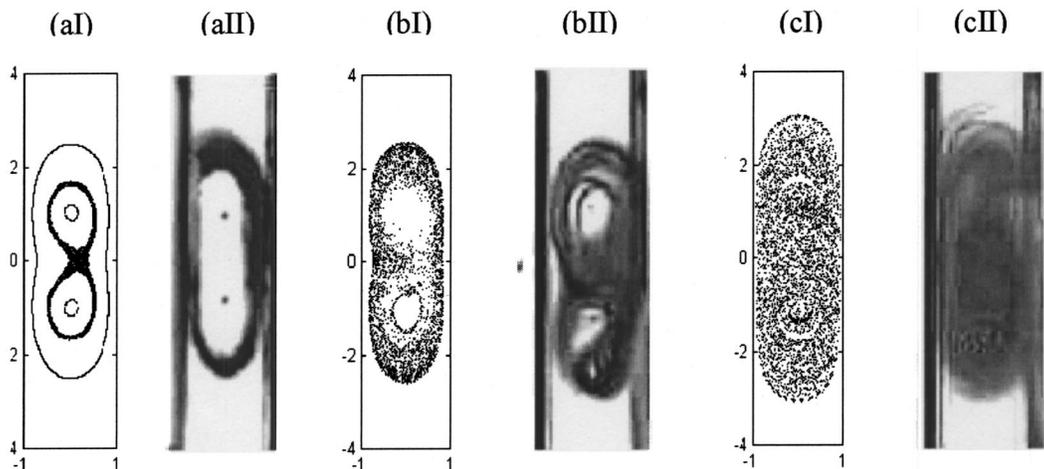

FIG. 9. Stroboscopic image (I) and flow visualization photos (II) when two (co-rotating) electrode groups are engaged. $c=1$ and $T_1=T/2$. (a) $T=4$; (b) $T=8$; (c) $T=20$.

straight conduits' bottoms. The ''point'' electrodes were positioned at various distances apart to facilitate the examination of the effect of the interelectrode distance on the nature of the flow. In the upper conduit, the ''point'' electrodes were positioned at distances ± 4 mm ($A_{\pm 1}$) and ± 10 mm ($A_{\pm 2}$) from the central electrode (A_0). In the lower conduit, the ''point'' electrodes were positioned at distances ± 2 and ± 6 mm from the conduit's midlength. All the electrodes were connected via computer-controlled relay actuators and a D/I card (PCL-725, Advantech Co., Ltd.) to the terminals of two dc-power supplies (Hewlett Packard, HP 6032A). The relays were wired and programmed to switch ''on'' and ''off'' each of the electrodes. The device was positioned on top of a neodymium (NdFeB, Polymag Inc.), permanent magnet that provided a magnetic field of $B \sim 0.4$ T. The cavity was filled with 0.36 M $\pm 10\%$ saline solution with a conductivity of $\sigma = \sim 3.9 \, \Omega^{-1} \, m^{-1}$. Since the magnitude of the Lorentz force is dictated by the intensity of the current, the solution's conductivity merely determines the potential difference needed to obtain the desired current.

After inserting the saline solution in the stirrer, we measured the current in the device as a function of the potential difference between electrodes A_0 and C (Fig. 8). The measurements were carried out for 0.1 M (A) and 0.36 M (B) saline solutions. Witness that there is a potential difference threshold (V_0) such that beneath the threshold value little current passes in the solution. Once the potential difference increases above the threshold, the current increases nearly linearly with the potential difference. We conducted all our experiments at currents well below 5 mA. When the current's magnitude was increased above ~ 6 mA, we observed significant formation of bubbles next to the electrodes.

When the device operated in a ''pumping'' mode, a potential difference was imposed across the electrode pair C^+ and C^-, and liquid circulated around the device. When the device operated in a ''stirrer'' mode, the two wall electrodes were connected together to act in tandem as a single electrode C, and the potential difference alternated between various A_n and C. In our experiments, the alternation period ranged from 1 to 10 s. We varied the effective (dimensionless) period, T, by varying both the potential-difference across the electrodes and the actual (dimensional) period.

The flow field was visualized by introducing a drop of dye (Fluorescent Liquid Dye, Cole-Parmer Instrument Company) at various locations inside the channel. Because of equipment limitations, the flow visualization allowed us to obtain only a crude qualitative description of the flow field. The images of the flow field were captured with both video and still cameras. The movies provide a much more vivid account of the evolution of the dye tracers.[18]

In our experiments, we did not observe any significant bubble generation. This is consistent with the very low electrical currents transmitted through the apparatus. Over time, however, the electrodes degraded. This could be a problem in a practical device designed to operate for an extended period of time. The erosion problem can be significantly reduced or even eliminated by appropriate selection of electrode material and electrolyte solution and/or through the use of an ac electric field. By appropriate synchronization of an ac electromagnetic field with an ac current, the direction of the Lorentz force would remain unaltered.[4]

V. CHAOTIC ADVECTION

The stirring process depends on a number of parameters such as the electrodes' locations, the number of electrode groups engaged, the protocol for time variation, and the period of the time alternations. Here, we provide a sample of our computations and experimental observations. We consider the cases of two and three alternating agitators (electrode groups) with distance $c = h$ between any two adjacent
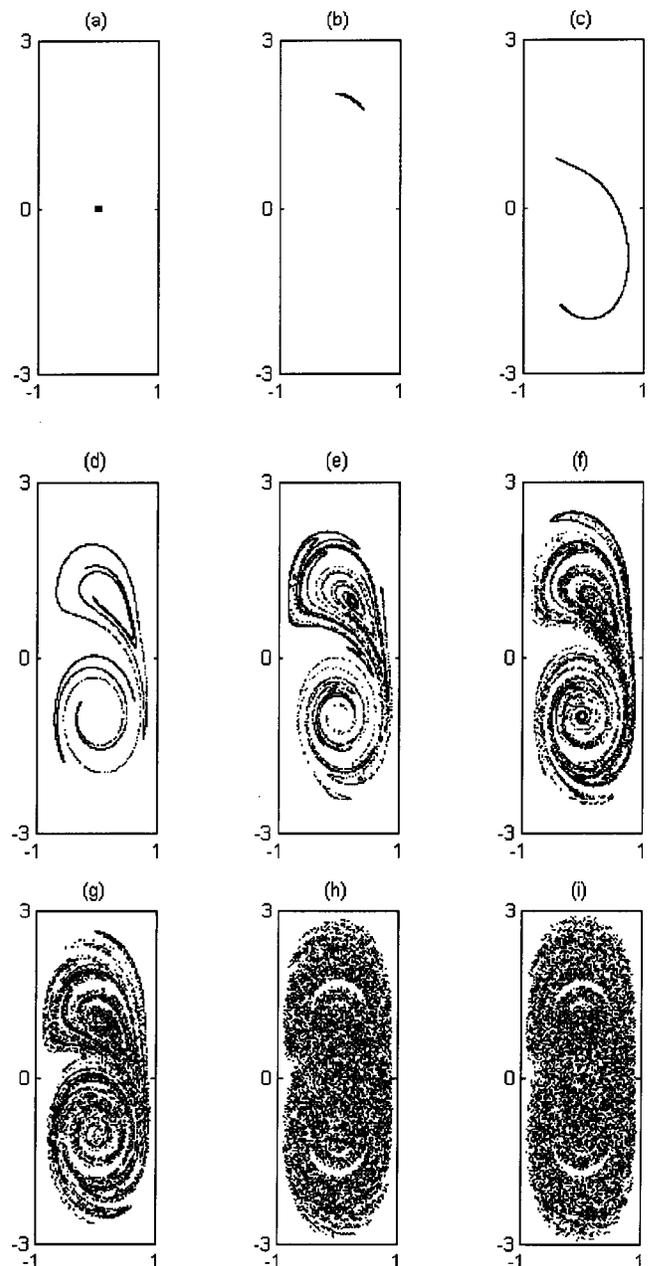

FIG. 10. Deformation of a material blob alternately excited by two electrode groups. Co-rotating, $c = 1$ and $T = 20$. (a) $t = 0$; (b) $t = T$; (c) $t = 2T$; (d) $t = 3T$; (e) $t = 4T$; (f) $t = 5T$; (g) $t = 6T$; (h) $t = 15T$; and (i) $t = 20T$.
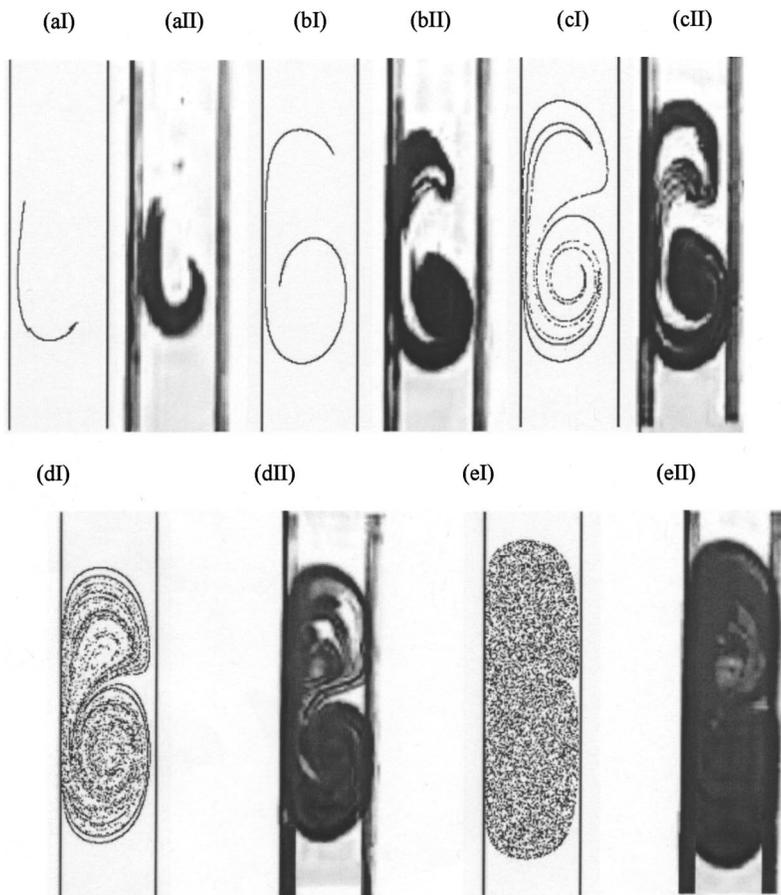
FIG. 11. Deformation of a material blob alternately excited by two agitators. Counter-rotating, $c=1$ and $T=20$. I and II represent, respectively, the computational results and the visualization photos. (a) $t=2T$; (b) $t=3T$; (c) $t=4T$; (d) $t=6T$; (e) $t=20T$.

A_n electrodes. When two or three agitators are engaged, we set, respectively, $T_1=T/2$ and $T_1=T_2=T/3$. We use the flow visualization experiments to illustrate that qualitatively similar phenomena to that predicted occur in the experiments. The period T in the experiment is an approximation of the theoretical value.

Figure 9 depicts the stroboscopic images (Poincaré sections) of a passive tracer (I) and flow visualization observations (II) when two agitators induce co-rotating motions and $T=4$ (a), 8 (b), and 20 (c). The stroboscopic images (I) were obtained by integrating Eq. (13) and documenting the tracer's location at the end of each period. The equations were integrated for 5000 periods and the tracer particle(s) were initially injected at {0, 0}, {0, ±0.9} and {0, 2.5} [Fig. 9(a)] and {0, 0} [Figs. 9(b) and 9(c)]. In the experiments, a drop of dye was initially inserted at approximately {0, 2} [Fig. 9(aII)], and {0, 0} [Figs. 9(bII) and 9(cII)]. When the period (T) is relatively small [Fig. 9(aI)], only narrow regions of irregularity are observed. Both the theoretical and experimental data illustrate that at relatively small periods, the flow has a similar structure to the "superposed" flow topology observed in the limiting case of $T\rightarrow0$. As T increases [Fig. 9(b)], so does the size of the chaotic region and the spread of the dye. When $T=20$ [Fig. 9(c)], the chaotic region has nearly occupied the entire region $-3<y<3$.

Another way to examine the stirring process is to track the history of a material blob inserted into the liquid. To this end, we inserted a square material blob of edge size 0.1, centered at (0, 0), and tracked its evolution as a function of time by integrating the trajectories of 10^4 points initially evenly distributed within the square. Figure 10 depicts the evolution of the blob at times $t=0$ (a), T (b), $2T$ (c), $3T$ (d), $4T$ (e), $5T$ (f), $6T$ (g), $15T$ (h), and $20T$ (i) when $T=20$ and co-rotating agitators. Figure 10 illustrates the rapid stretching and folding processes associated with chaotic advection. At time $t=6T$, the trace particles have visited most of the mixing region, allowing diffusion (absent in Fig. 10) to complete the mixing process.

For the case of $T=20$ and two counterotating agitators, Fig. 11 depicts the evolution of a square material blob of edge size 0.1, centered at (0, 0), as a function of time by integrating the trajectories of 10^4 points initially evenly distributed within the square. Figure 11 compares qualitatively the computational results with experimental observations. Due to the rapid stretching process, we believe that the differences in the blob's initial shape in the experiment and theory should have only a minor effect on the blob's evolution. Figure 11 depicts the blob's evolution at times $t=2T$ (a), $3T$ (b), $4T$ (c), $6T$ (d), and $20T$ (e). More complicated motions can be produced when more than two agitators are engaged.

VI. CONCLUSIONS

The paper describes a low Reynolds number, novel magnetohydrodynamic stirrer that can be used in minute fluidic devices in general and in magnetohydrodynamic fluidic circuits in particular. The MHD circuit consists of individually controlled branches. With appropriate adjustment of potential differences across electrodes, each of the network branches can double as a stirrer. Neither the MHD circuit nor the stirrer requires any mechanical parts. The pumping and stirring functions are achieved by judicious interplay between magnetic and electric fields to generate Lorentz forces in any desired direction. When network branches are operating as stirrers, potential differences are alternately applied between inner and wall electrodes. Each stirrer is equipped with two or more agitators. By alternately actuating the agitators, we demonstrate both in experiment and theory that it is possible to induce chaotic advection and efficient stirring. The theoretical results are in good qualitative agreement with experimental observations. This is yet another practical example of a system that exhibits chaotic advection in the Stokes flow regime. Moreover, this investigation illustrates a way of constructing inexpensive laboratory experiments that exhibit complex flow behaviors.

Unfortunately, the operation of the MHD fluidic network and stirrer is not completely problem-free. Some potential problems are bubble formation, electrode consumption, and migration of analytes in the electric field. The severity of these undesired phenomena depends on the device's configuration and its length of operation. For example, bubble formation is not likely to be a problem when one operates for relatively short time intervals or with open trenches. Moreover, it does not appear to be a problem at very low potential differences. Electrode erosion is not likely to be of concern in disposable devices. Furthermore, the adverse effects of bubble generation, electrode consumption, and charged molecules migration could be greatly reduced by operating with synchronized, alternating magnetic and electric fields (i.e., the various electrodes assume alternately the roles of cathodes and anodes) and/or by judicious selection of the analyte solution. Finally, the electrodes can be passivated to reduce their erosion.

[1] H. H. Woodson, and J. R. Melcher, *Electromechanical Dynamics* (Wiley, New York, 1969), Vol. III.

[2] P. A. Davidson, *An Introduction to Magnetohydrodynamics* (Cambridge University Press, Cambridge, 2001).

[3] J. Jang and S. S. Lee, ''Theoretical and experimental study of MHD (magnetohydrodynamic) micropump,'' Sens. Actuators A **80**, 84 (2000).

[4] A. V. Lemoff and A. P. Lee, ''An ac magnetohydrodynamic micropump,'' Sens. Actuators B **63**, 178 (2000).

[5] J. Zhong, M. Yi, and H. H. Bau, ''Magnetohydrodynamic (MHD) pump fabricated with ceramic tapes,'' Sens. Actuators A **96**, 59 (2002).

[6] H. H. Bau, ''A case for magnetohydrodynamics (MHD),'' IMECE 2001, MEMS 23884 Symposium Proceedings, New York, 2001.

[7] H. H. Bau, J. Zhong, and M. Yi, ''A minute magnetohydrodynamic (MHD) mixer,'' Sens. Actuators B **79**, 205 (2001).

[8] M. Yi, S. Qian, and H. H. Bau, ''A magnetohydrodynamic chaotic stirrer,'' J. Fluid Mech. (in press).

[9] H. Aref, ''Stirring by chaotic advection,'' J. Fluid Mech. **143**, 1 (1984).

[10] W. W. Hackborn, M. E. Ulucakli, and T. Yuster, ''A theoretical and experimental study of hyperbolic and degenerate mixing regions in a chaotic Stokes flow,'' J. Fluid Mech. **346**, 23 (1997).

[11] L. D. Landau and E. M. Lifshitz, *Fluid Mechanics* (Pergamon, Oxford, 1959).

[12] P. Moon, and D. E. Spencer, *Field Theory Handbook* (Springer, Berlin, 1971).

[13] W. W. Hackborn, ''Asymmetric Stokes flow between parallel planes due to a rotlet,'' J. Fluid Mech. **218**, 531 (1990).

[14] H. K. Moffatt, ''Viscous and resistive eddies near a sharp corner,'' J. Fluid Mech. **18**, 1 (1964).

[15] H. Aref and S. Balachandar, ''Chaotic advection in Stokes flow,'' Phys. Fluids **29**, 3515 (1986).

[16] J. Chaiken, C. K. Chu, M. Tabor, and Q. M. Tan, ''Lagrangian turbulence and spatial complexity in Stokes flow,'' Phys. Fluids **30**, 687 (1987).

[17] H. H. Bau, G. K. Ananthasuresh, J. J. Santiago-Aviles, J. Zhong, M. Kim, M. Yi, and P. Espinoza-Vallejos, ''Ceramic tape-based meso systems technology,'' Micro-Electro-Mechanical Systems (MEMS), DSC-Vol. 66, 491 (1998).

[18] A sample video clip is available at http://www.seas.upenn.edu:8080/~bau/ MHD%20Chaotic%20Stirrer.mov